Computing the effects of excitatory-inhibitory balance on neuronal input-output properties

Alex Reyes

Center for Neural Science, New York University, New York, NY USA

Abstract

In sensory systems, stimuli are represented through the diverse firing responses and receptive fields of neurons. These features emerge from the interaction between excitatory and inhibitory neuron populations within the network. Changes in sensory inputs alter this balance, leading to shifts in firing patterns and the input-output properties of individual neurons and the network. While these phenomena have been studied extensively with experiments and theory, the underlying principles for combining E and I inputs are still unclear. Here, rules for probabilistically combining E and I inputs are derived that describe how neurons in a feedforward inhibitory circuit respond to stimuli. This simple model is broadly applicable, capturing a wide range of response features that would otherwise require multiple separate models and offers insights into the cellular and network mechanisms influencing the input-output properties of neurons, gain modulation, and the emergence of diverse temporal firing patterns.

Introduction

A common motif in the sensory systems is the feedforward inhibitory circuit, where excitatory afferents from an external source synapse onto both excitatory (E) and inhibitory (I) neurons, with inhibitory neurons then synapsing back onto E cells [1, 2, 3, 4, 5]. During stimulation, interactions within this circuit generate complex dynamics and shape the receptive field properties of neurons. As stimulus parameters vary, the balance between E and I inputs shifts, leading to both qualitative and quantitative changes in neuronal sensitivity and evoked firing patterns [1, 4, 6, 7].

A neuron's response to a stimulus is characterized by its input–output (I–O) curve, where the input typically refers to synaptic current and the output to firing rate. Compared to neurons *in vitro* [8, 9], neurons *in vivo* exhibit more diverse I-O profiles. Background excitation and inhibition from ongoing network activity introduce membrane potential fluctuations, allowing neurons to respond even to weak inputs that would otherwise remain subthreshold, and to generate smoothly increasing I–O curves [10, 11, 12, 13]. In some cases, responses initially increase with stimulus intensity but then decline after reaching a peak [14, 15, 16, 17], likely due to strong inhibitory recruitment [18, 19]. I–O curves also depend stimulus duration: brief stimuli (5–50 ms) evoke responses sensitive to the timing of excitation and inhibition [2, 4, 20, 21], while longer stimuli (hundreds of milliseconds) evoke responses that vary with the average synaptic current generated during barrages [22, 23, 24].

Moreover, the I-O curves may change depending on the animal's state, such as when it is at rest, in motion [25, 26] or actively attending [27, 28]. To maintain selectivity to stimulus features across states, the slope of the I-O curve should change without affecting the minimum input needed to evoke firing [13, 29]. This multiplicative (or divisive) gain modulation can arise from feedback from neighboring E and/or I neurons [30, 31, 32, 33, 34], feedforward inhibition [21] or the combination of synaptic noise and conductance [10]. Additive (or subtractive) modulation, by contrast, shifts the activation threshold without altering gain, thereby affecting tuning curve width [13].

Finally, differences in E -I balance can produce diverse temporal firing responses. Some neurons exhibit continuous firing throughout the stimulus duration, while others fire transiently at the stimulus onset [16, 22, 35, 36, 37, 38, 39] and/or at the offset [39, 40, 41, 42] . These firing profiles are observed in cortical and subcortical neurons [42] and may be generated locally [22, 41, 42, 43, 44] or inherited from upstream sources [40]. Additionally, a neuron's response type may change based on the stimulus intensity [16] or whether the preferred stimulus is presented [35, 38, 45, 46].

Identifying common operating principles across these phenomena will provide valuable insights into potential mechanisms. This study aims to derive rules for calculating E-I balance in feedforward inhibitory circuits. The model combines E and I inputs probabilistically and links the associated changes in responses and I-O curves to the synaptic and network properties. The model reproduces and clarifies the conditions for gain modulation, non-monotonic I-O curves, and diverse firing patterns.

Results

The circuit examined here is a feedforward inhibitory circuit in which both E and I neurons receive excitatory synaptic inputs from an external source, with the I neurons providing inhibitory inputs to the E neurons. The following sections first introduce core concepts using an idealized network, then extend them to more physiologically realistic scenarios.

Consider a hypothetical circuit where a postsynaptic neuron receives a single, suprathreshold excitatory postsynaptic potential (EPSP) from an external source and an equally large inhibitory postsynaptic potential (IPSP) from an inhibitory interneuron (Fig. 1A). During a stimulus, the EPSP and IPSP appear in the cell independently with no delay and with equal probabilities p_E and p_I, respectively. An action potential is elicited each time the EPSP occurs but can be canceled by the IPSP. Even with identical parameters , the neuron will still fire as long as $p_E \neq 0$ and $p_I \neq 1$. In Fig. 1A, 4 EPSPs (blue) and 4 IPSPs (red) appear over 7 trials. Only IPSPs coinciding with the EPSPs affect firing (trials 3 and 6): trials where the IPSP either failed to appear (trials 1 and 4) or appeared by itself (trials 2 and 7) does not decrease firing. Hence, the firing probability p_f may be expressed as:

$$\begin{aligned} p_f &= p_E - p_E p_I \\ &= p_E(1 - p_I) \end{aligned} \tag{1}$$

where $p_E p_I$ reflects the probability that the EPSPs and IPSPs occur coincidentally.

The surface plot in Fig 1A shows how p_f varies with p_E and p_I, highlighting key properties of eq.1. First, p_f is non-zero even if p_E and p_I are equal except when p_E =0 or p_I =1. Second, p_f depends on how p_E and p_I co-vary. If p_I increases with p_E at different rates (e.g. $p_I = k_c p_E, 0 \leq k_c \leq 1$), p_f increases monotonically for small k_c but non-monotonically for larger k_c (orange curves). Third, if p_I is fixed, p_f increases linearly with p_E at different rates (slope = $(1 - p_I)$; green curves). The inset shows the orange and blue curves projected to the p_f vs p_E plane, representing the 'input-output' (I-O) relation of the neuron where p_E serves as a proxy for stimulus intensity.

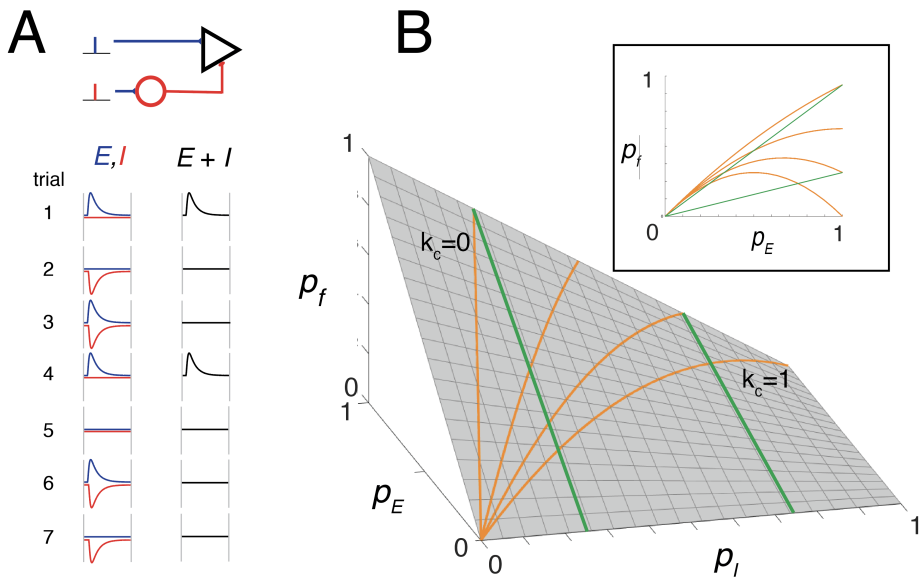

Figure 1: Toy model illustrating basic principles. **A,top**, schematic of a simple feedforward inhibitory circuit. A postsynaptic excitatory neuron (black triangle) and a local inhibitory interneuron (red circle) both receive a single, suprathreshold excitatory input from an external source. An IPSP is generated in the postsynaptic excitatory neuron whenever the interneuron fires. **Bottom**, EPSPs (blue) and IPSPs (red) evoked in the postsynaptic E neuron over 7 trials. The IPSP cancels the EPSP only if it appears simultaneously. **B**, surface plot of firing probability p_f as a function of p_E and p_I. Orange curves show predicted firing probability when p_I increases linearly with p_E ($p_I = k_c p_E$) at different rates. Green curves are with p_I held constant. Inset, the curves are projected to the p_f vs p_E plane.

General model

The responses of neurons depend in part on the duration of the sensory input. During prolonged stimulation, the excitatory afferents and inhibitory neurons generate sequences of EPSPs and IPSPs, respectively, creating a synaptic barrage in the postsynaptic, excitatory neuron (henceforth termed 'reference' neuron). If the input is sufficiently strong, neurons fire repetitively, at a rate that depends on the average synaptic current [23]. In contrast, brief stimuli result in near synchronous arrival of EPSPs and IPSPs, placing the neuron in a regime where spiking is more sensitive to the amplitude and precise timing of synaptic inputs [4]. These distinct regimes will be addressed separately, as the model yields different predictions for each.

Long stimuli: oscillatory firing regime

In this configuration, external afferents fire at a rate r_E during stimulation, generating excitatory inputs to both the reference cell and inhibitory neurons with time-dependent probabilities $p_E(t)$ and $p_{E\to I}(t)$, respectively (Fig. 2A). The inhibitory neurons then fire at at rate r_I, and inhibitory barrages appear in the reference neuron with probability $p_I(t)$. As discussed earlier, only inhibitory inputs that are co-activated with the excitatory input contribute to the reference neuron's firing. The probability of this co-activation is given by the product $p_E(t) \cdot p_I(t)$. Taking into account the number of excitatory afferents (n_E), their firing rate (r_E), and the charge delivered per input (q_E), along with the corresponding parameters for inhibitory inputs (n_I, r_I, q_I), the net synaptic current is (see appendix S1):

$$\begin{aligned} i_{net}(t) =& q_E n_E r_E p_{net}(t) \\ p_{net}(t) =& p_E(t)(1 - k_n k_q k_r p_I(t)); 0 \leq k_n k_q k_r \leq 1 \end{aligned} \tag{2}$$

where $k_n = \frac{n_I}{n_E}, k_q = |\frac{q_I}{q_E}|$ and $k_r = \frac{r_I}{r_E}$. The value of k_n is set to 0.2, consistent with the ratio observed in the cortex [47, 48], while k_q is set to 1 [2, 49], under the assumption that synaptic potentials are voltage-independent (the case with conductance-based synapses is addressed below). The parameter k_r depends on the inhibitory firing rate r_I, which varies with stimulus intensity.

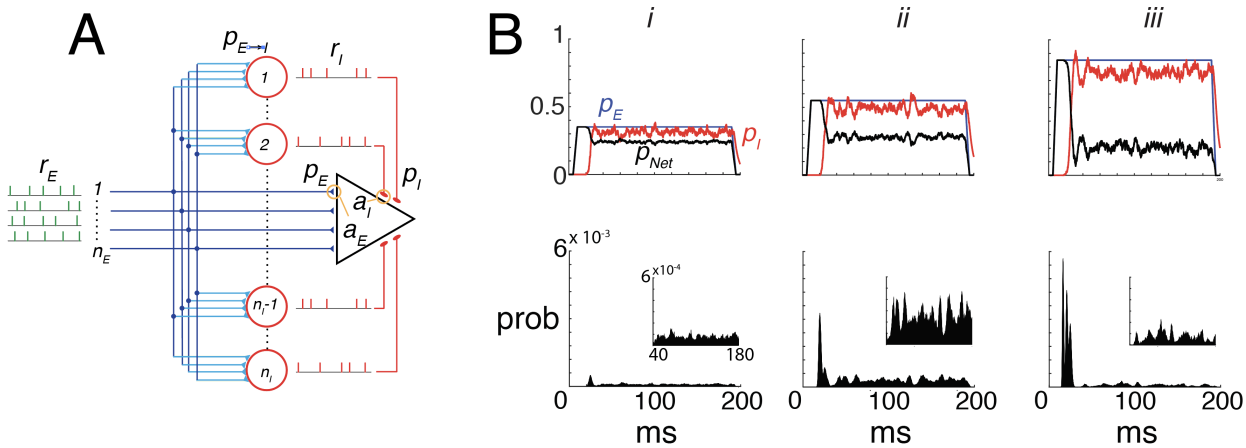

Figure 2: Predicting firing rate in response to sustained stimuli. **A**, Schematic of the network, consisting of a reference cell (triangle) and $n_I = 50$ inhibitory neurons (red circles). All neurons receive input from $n_E = 250$ excitatory afferents, each firing at a rate $r_E = 50$ Hz. During stimulation, excitatory trains arrive at the reference cell with probability p_E, and at the inhibitory neurons with probability $p_{E\to I}$. Each inhibitory neuron fires repetitively at a rate $r_I \approx$ 20–100 Hz with probability p_I, producing IPSP trains in the reference cell. The amplitude of EPSPs (a_E) and IPSPs (a_I) are 250 and -250 μV, respectively, corresponding to unitary charges of $q_E = 0.0557$ and $q_I = -0.0557\,pS$. Simulations used leaky-integrate-fire neurons (see Methods). **B*i*, top**, Time course of excitatory input probability $p_E(t)$ (blue), which ramps to a steady-state value of 0.5. Inhibitory input probability $p_I(t)$ (red) follows after a delay of approximately 20 ms. The resulting net probability $p_{\text{net}}(t)$ (black) shows a transient peak at stimulus onset followed by a lower steady-state level. **Bottom**, Spike histogram of the reference neuron. **Inset**, magnified view of the tonic component of the firing. ***ii, iii***, Same as in ***i***, except $p_E(t)$ ramps to steady-state values of 0.75 and 1.0, respectively.

In Fig. 2B, simulations were performed using Leaky-Integrate-and-Fire (LIF) neurons (see figure caption and Methods for details). The afferent probability $p_E(t)$ was ramped up to a steady level (Fig. 2B,*i–iii*, top panels, blue), resulting in a rapid rise of $p_I(t)$ after a short delay (red). Both the computed $p_{\text{net}}(t)$ (black) and the firing rate profile of the reference cell (bottom panel) exhibited a peak at onset followed by a tonic component. Under these stimulus conditions, the phasic component was due to the lag in inhibition; however, it can still occur even when $p_E(t)$ and $p_I(t)$ follow identical time courses (see below). The tonic firing reflected the balance between $p_E(t)$ and $p_I(t)$, consistent with the toy model. As both probabilities increased, the tonic firing initially rose to a peak value (*ii*, inset) and then declined (*iii*), eventually vanishing as the probabilities approached 1 (see below for a more general treatment).

Plotting the firing rate vs the mean, steady-state probability ($\bar{p}_E$) yields the I-O curve (Fig.3A). When the net input current i_{net} exceeded the rheobase i_{rh}, the neuron entered the oscillatory firing regime, with the average firing rate of a LIF neuron (green curve) given by

$$r_{osc} = [(\tau_m * ln(\frac{\bar{i}_{net}}{\bar{i}_{net} - i_{rh}})]^{-1} \tag{3}$$

where $\bar{i}_{net}$ is the mean, steady-state net current and τ_m is the membrane time constant. However, firing can still occur with weak inputs due to intrinsic current fluctuations occasionally surpassing i_{rh}, even when $\bar{i}_{net}$ is low (Fig. 3A, left inset). The firing rate in this sub-oscillatory, or fluctuation-dominated regime, (A, cyan,) is given by (see appendix S1):

$$r_{\text{fluct}} = r_{rh} \cdot \text{prob}(\bar{i}_{net} > i_{rh}) \tag{4}$$

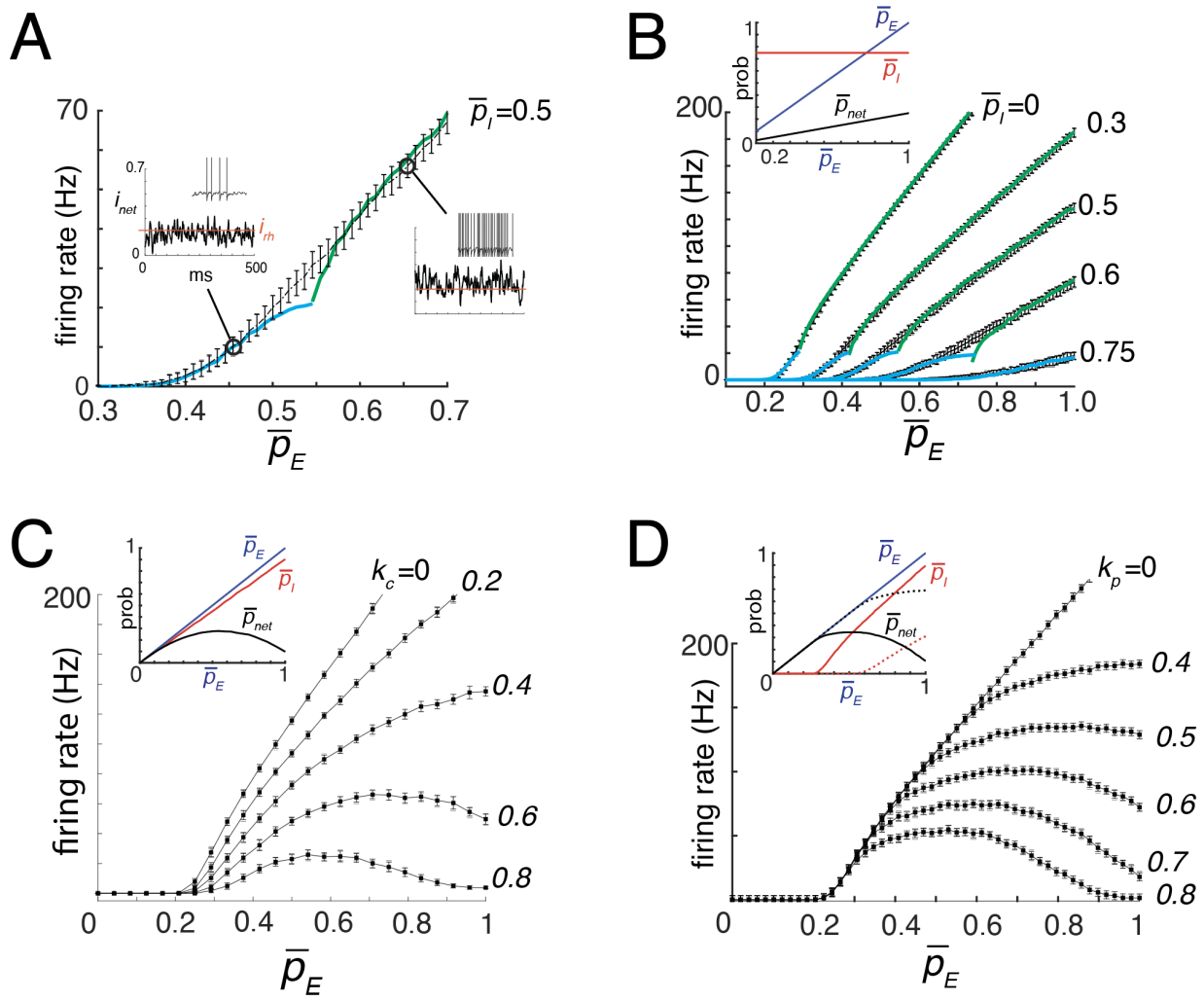

Figure 3: Gain modulation of Input-output curves. **A**, representative I-O curve (plot of mean firing rate (+/- SD) vs $\bar{p}_E$) with $\bar{p}_I$ set to 0.5. Superimposed are the predicted firing in the sub-oscillatory (cyan) and oscillatory regimes (green). **Inset**, synaptic current and associated firing generated with small (left) and large (right) $\bar{p}_E$ values. Orange line is rheobase . **B**, I-O curves for different fixed values of $\bar{p}_I$. **Inset**, plot of $\bar{p}_E$,$\bar{p}_I$, and $\bar{p}_{net}$vs $\bar{p}_E$. **C**, same, except $\bar{p}_I$increased linearly with $\bar{p}_E$as $\bar{p}_I = k_c\bar{p}_E$. To vary $k_c(= k_n k_q k_r)$, k_n was adjusted while keeping k_q, k_r fixed. **D** , same, except $\bar{p}_{E\to I}$ increased linearly with $\bar{p}_E$as $\bar{p}_{E\to I} = k_p\bar{p}_E$. **inset**, $\bar{p}_I$increased linearly with $\bar{p}_E$past threshold. Solid and dotted curves are with $k_p = 0.7, 0.4$, respectively.

where r_{rh} is the minimum oscillatory firing rate at i_{rh} and prob($i_{net} > i_{rh}$) is computed using a binomial cumulative distribution function. The increase of r_{fluct} with $\bar{p}_E$ follows an S-shaped curve, asymptotically approaching a peak value near the onset of the oscillatory regime. The firing rate for the entire range of p_E is then the larger of r_{fluct} and r_{osc}.

The model predicts that for a fixed p_I, the slope of the I-O curve will change in proportion to $1 - p_I$ (Fig. 1B, green and eq. 1). To test this, the input probability to inhibitory neurons ($p_{E\to I}$; Fig. 2A) was adjusted to maintain a constant average inhibitory probability $\bar{p}_I$ with increasing $\bar{p}_E$ (Fig. 3B, inset). This simulates the sustained recruitment of inhibitory neurons during sensory stimulation, replicated experimentally with continuous optogenetic activation of I neurons [34]. As $\bar{p}_I$ increased, the I-O curves exhibited a decrease in slope and a rightward shift, indicating a higher threshold for activation. This threshold shift reflects persistent inhibition across the full range of $\bar{p}_E$ (inset), requiring stronger excitation to elicit firing. These slope changes occurred in both the oscillatory and sub-oscillatory regimes and were predicted by the equations for r_{osc} (green) and r_{fluct} (cyan). The combined changes in slope and threshold demonstrate that inhibition in this case modulates the I-O curve through both multiplicative and additive mechanisms [13, 29].

The I-O curves exhibited either monotonic or non-monotonic increases with $\bar{p}_E$, depending on how strongly inhibition co-varied with excitation, consistent with model predictions (Fig. 1B, orange curves). Fig. 3C shows the mean (+/- SD) firing rate as $\bar{p}_I$ increased linearly with $\bar{p}_E$ at different rates ($\bar{p}_I = k_c\bar{p}_E; 0 \leq k_c = k_n k_q k_r \leq 1$; inset). For small k_c, firing rates increased monotonically with $\bar{p}_E$. As k_c approached 1, the curves flattened and eventually became non-monotonic. Notably, the minimum value of $\bar{p}_E$ required to evoke firing (approximately 0.2) remained unchanged, while the slope of the rising phase decreased. Therefore, when $\bar{p}_E$ is restricted to the range where the I–O curve is increasing, gain modulation is effectively multiplicative.

The model also predicts changes in I-O curves under more physiological conditions where $\bar{p}_I$ follows the I-O profile of the I neurons. To simulate this, $\bar{p}_{E\to I}$ was set to increase linearly with $\bar{p}_E$ ($\bar{p}_{E\to I} = k_p\bar{p}_E$, with $0 \leq k_p \leq 1$). As a result, the firing rate of I neurons and the associated $\bar{p}_I$ was zero at low $\bar{p}_E$ and then rose linearly beyond a threshold (Fig. 3D, inset). As k_p increased, the $\bar{p}_I$ curve shifted leftward (dotted red line to solid red line in inset), which in turn made the I–O curves of the reference neuron increasingly non-monotonic. The I-O curves had identical thresholds and overlapped before diverging. While these changes do not conform to standard forms of gain modulation, they can still produce multiplicative effects on tuned input (see below).

Correction for conductance effects

A key assumption in deriving eq. 2, is that the excitatory and inhibitory inputs sum linearly, which is not generally the case as synaptic inputs can induce conductance changes. Consequently, the net current calculated at rest can differ substantially from that during active states when the membrane potential is depolarized, leading to significant errors in firing rate estimates. To correct for this, a conductance-dependent adjustment term is derived (see appendix S1). Including this correction significantly improves the accuracy of firing rate predictions, closely aligning them with simulation results (Fig. S1).

Gain modulation of tuned responses

The slope changes in the I-O curves above (Figs. 3B-D), suggest mechanisms for multiplicative gain modulation of neural responses [27, 28, 50]. To test this, simulations were performed with $\bar{p}_E$ following a Gaussian profile representing tuned sensory input (Fig. 4A). This was delivered to the network under 3 conditions: with fixed $\bar{p}_I$ (mode 1), $\bar{p}_I$ increasing linearly with $\bar{p}_E$ (mode 2), or

with $\bar{p}_I$ following the I-O curve of the I neurons (mode 3). In all cases, the peak input ($\bar{p}_E = 0.35$) yielded modulated tuning curves with peak firing rates within 50% of the control (60 Hz), consistent with experimental data [27, 28, 50].

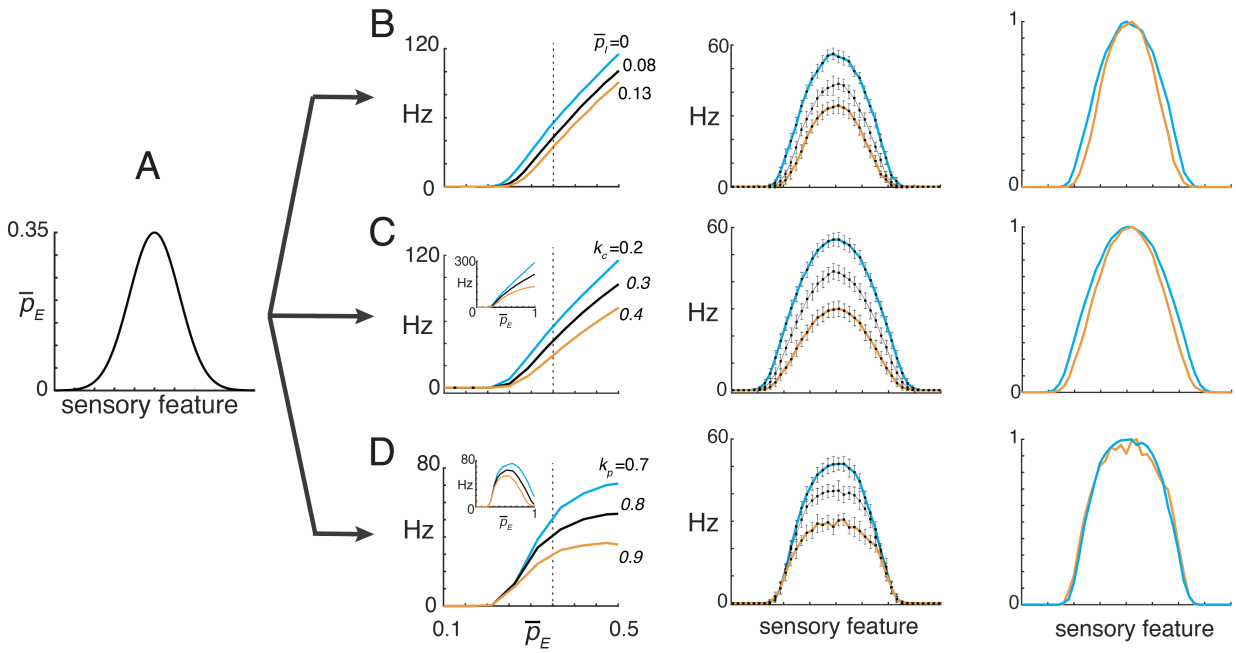

Figure 4: Gain modulation of tuned responses. **A**, simulations were performed where $\bar{p}_E$ followed a Gaussian curve representing tuned sensory input. **B,top**, The I-O curves used to transform the input. The values of $\bar{p}_I$were held constant. **Middle**, tuned responses of the reference neuron. **inset**, I-O curves across the full range of $\bar{p}_E$. **Right**, tuned responses normalized to a peak value of 1. **C**, same except $\bar{p}_I$ increased linearly with $\bar{p}_E$ as $\bar{p}_I = k_c\bar{p}_E$. **D**, same except $p_{E\to I}$ increased with p_E as $p_{E\to I} = k_p p_E$.

For mode 1, relatively small values of $\bar{p}_I$ ($= 0, 0.08, 0.13$) were sufficient to produce multiplicative gain modulation. Although the I-O curves showed both slope and threshold changes (Fig. 3B), the small range of $\bar{p}_I$ that was used primarily affected the slope (Fig. 4B, left), resulting in a reduction in tuning curve amplitude (middle) with minimal change in width (right). Physiologically, such low $\bar{p}_I$ values, which is scaled by $k_n k_q, k_r$ (eq. 2), could arise from a small number of inhibitory neurons relative to afferents (low k_n), weak synaptic inhibition (low k_q), and/or low inhibitory firing rates (low k_r).

In mode 2, multiplicative gain modulation was achieved by setting the scalar k_c in the relationship $\bar{p}_I = k_c\bar{p}_E$ to modest values of 0.2, 0.3, and 0.4. The resulting I-O curves were monotonic with progressively reduced slopes as k_c increased (Fig. 4C, left and inset). The peaks of corresponding tuned responses (middle) varied with k_c and, when normalized, superimposed (right). To achieve a linear relationship between $\bar{p}_I$ and $\bar{p}_E$ under physiological conditions would require a fixed $p_{E\to I}$ across input intensities and a low inhibitory thresholds to ensure engagement even for small $\bar{p}_E$ values.

In mode 3, multiplicative gain modulation was achieved, but only for a limited range of $\bar{p}_E$. At low $\bar{p}_E$ values, the I–O curves overlapped substantially (Fig. 4D, left), requiring strong inhibition to induce divergence at moderate $\bar{p}_E$, where slope differences emerge. Under these conditions, the I–O curves are non-monotonic (inset). However, $\bar{p}_E$ must remain below the point where firing corresponds to the decaying edge of the I–O curve—exceeding this leads to a central dip and bimodal tuning curves (Fig. S2). When these conditions are satisfied, peak responses can be modulated (middle) with minimal changes in tuning width (right).

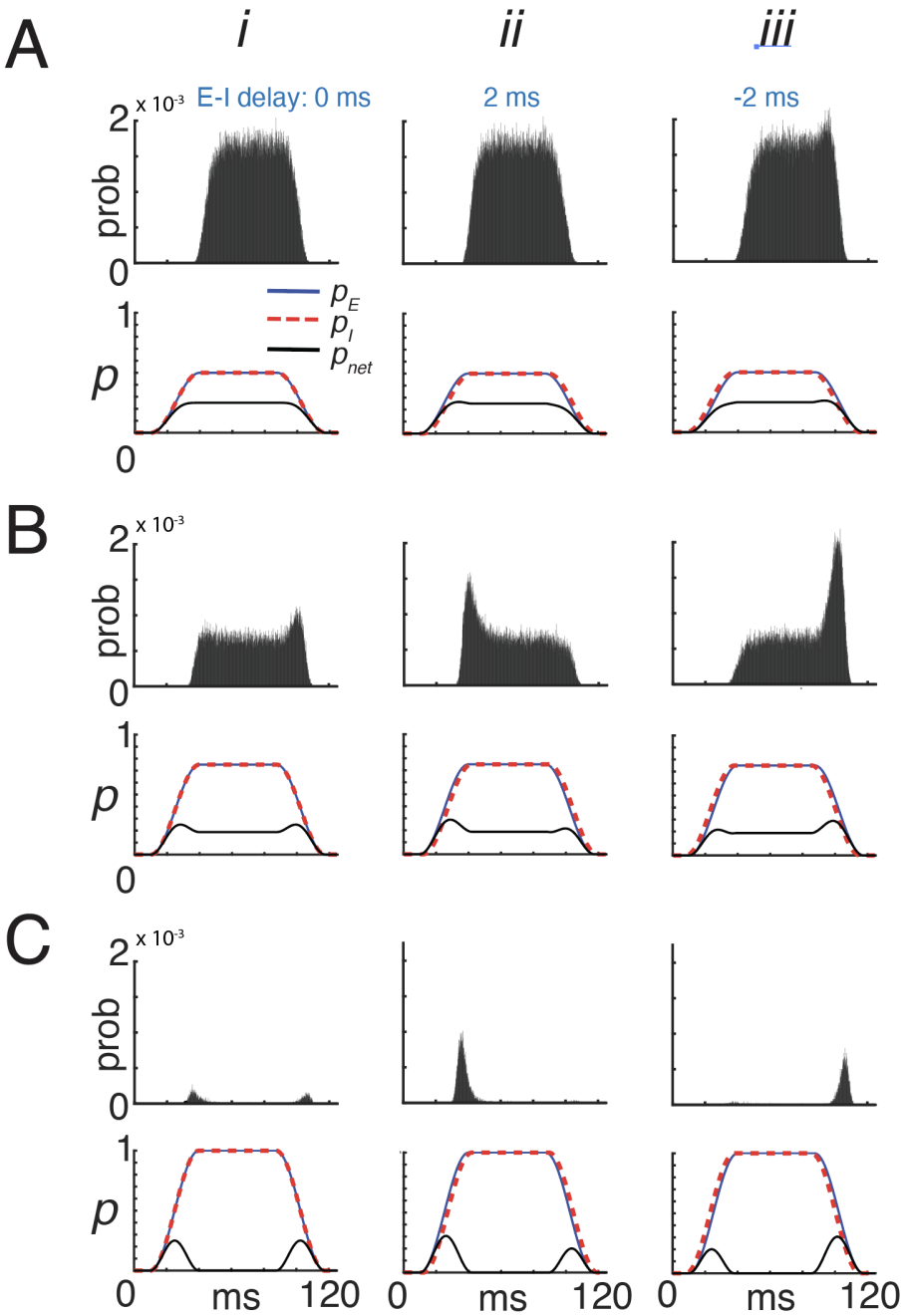

Figure 5: Effects of I magnitude and delay on spatiotemporal firing. **A*i*,bottom**, Excitatory and inhibitory input probabilities, $p_E(t)$ (blue) and $p_I(t)$ (red), tracked each other with no delay. Both reached a steady state level of 0.5. The computed $p_{net}(t)$ is superimposed (black). **Top**, Resulting spike histogram shows tonic firing in the reference neuron. ***ii-iii***, same except $p_I(t)$ lags or leads $p_E(t)$ by 2 ms. **B**, same as in **A** but with larger steady state values of probabilities (=0.75). **C**, same as in **(**A) but with steady state values equal to 1.

Temporal firing profiles

The temporal firing patterns of neurons can encode specific stimulus features or task-related components [36, 51, 52]. To investigate how these patterns depend on excitatory-inhibitory (E –I) interactions, it is essential to systematically vary the time-dependent input probabilities, $p_E(t)$ and $p_I(t)$. However, controlling the time course of $p_I(t)$ is difficult, as its onset and magnitude depend on how inhibitory neurons are recruited by the stimulus (Fig. 2B). This is dependent on the biophysical properties of the I neurons [53] and the amplitude of their E inputs [54, 55, 56]. Moreover, the reference cell's firing profile also depends on relative timing between EPSPs and IPSPs; in most cases, IPSPs lag behind EPSPs [2, 18, 40], though they may also precede them [49, 57]. Replicating the full range of possible $p_E(t)$ and $p_I(t)$ relationships would require detailed models of inhibitory neuron dynamics, which is beyond the scope of the present study. To allow for direct and independent control of $p_I(t)$, inhibitory neurons were bypassed, and inhibitory inputs were instead generated and delivered to the reference neuron in the same manner as excitatory afferents.

A wide range of temporal firing patterns can be generated by adjusting the magnitudes and timing of $p_E(t)$ and $p_I(t)$. In these simulations, the shapes of $p_E(t)$ and $p_I(t)$ are identical (Fig. 5A,B,C, bottom panels) but with different lags (*i*-*iii*). For moderate inputs with no lag (A,*i*), the computed $p_{net}(t)$ (black) followed the time courses of $p_E(t)$ (blue) and $p_I(t)$ (red dashed), ramping to a steady level and ramping back down. The reference neuron fired tonically after a delay (top). As the $p_E(t)$ and $p_I(t)$ magnitudes increased (B), the computed $p_{net}(t)$ had peaks at the onset and offset and a lower steady-state level. Further increases in steady-state amplitude (C) caused the tonic component to disappear entirely. The onset and offset peaks persisted because $p_E(t)\cdot(1-p_I(t)) \neq 0$ during those periods. Consequently, the reference neuron fired only at stimulus onset and offset (top panel).

Similar results were observed when $p_I(t)$ lagged $p_E(t)$ by 2 ms (*ii*), except that the onset peak of $p_{\mathrm{net}}(t)$ was larger than the offset peak (Fig. 5C). This resulted in pronounced firing at stimulus onset—greater than that observed in the no-delay condition (*i*)—and no firing at stimulus offset. In contrast, when $p_I(t)$ preceded $p_E(t)$ (*iii*), spiking occurred only at stimulus offset.

Transient firing regime

Brief stimuli, such as tone pips in the auditory system [49, 2, 33], light flashes in the visual system [58], or whisker deflections in the somatosensory system [6, 4], evoke a near-synchronous volley of compound EPSPs, followed by compound IPSPs from inhibitory neurons. Whether the postsynaptic cell fires depends both on the relative magnitude and timing of the EPSPs and IPSPs.

To examine the effects of E - I balance and timing on firing probability, simulations were performed in the same network as above but with 100 presynaptic afferents and 20 I neurons. During a stimulus, the active afferents generate EPSPs in the reference neuron with probability p_E and in the I neurons with probability $p_{E\to I}$. When the I neurons fire, they trigger IPSPs in the reference cell with probability p_I. EPSP arrival times follow a Gaussian distribution (Fig. 6A*i*, top panel, blue histogram) with the IPSPs appearing after some delay (red). The action potential distribution in the reference cell (middle, gray) is narrower than that of the afferent input, consistent with experimental data [4].

The firing probability of the reference cell in response to the input is calculated as follows. During stimulation, the time-varying probability that the membrane potential attains a particular value follows the time courses of the compound EPSPs and IPSPs. These are denoted as $\hat{p}_E(t)$ for excitation (Fig. 6A*i*, bottom panel, blue) and $\hat{p}_I(t)$ for inhibition (red), and are derived from the

temporal profiles of the summed EPSPs and IPSPs (see appendix S1). The net probability (black) is :

$$\hat{p}_{net}(t) = \hat{p}_E(t) \cdot (1 - k_n k_a \hat{p}_I(t)), 0 \leq k_n k_a \leq 1 \tag{5}$$
$$\hat{p}_x(t) = p_x \phi_x(t); x \in \{E, I\}$$

where $\phi(t)$ is the time course of the composite EPSP or IPSP, $k_n = \frac{n_I}{n_E}$ is the ratio of the number of inhibitory to excitatory inputs, and $k_a = |\frac{a_I}{a_E}|$ is the ratio of unitary IPSP to EPSP amplitude.

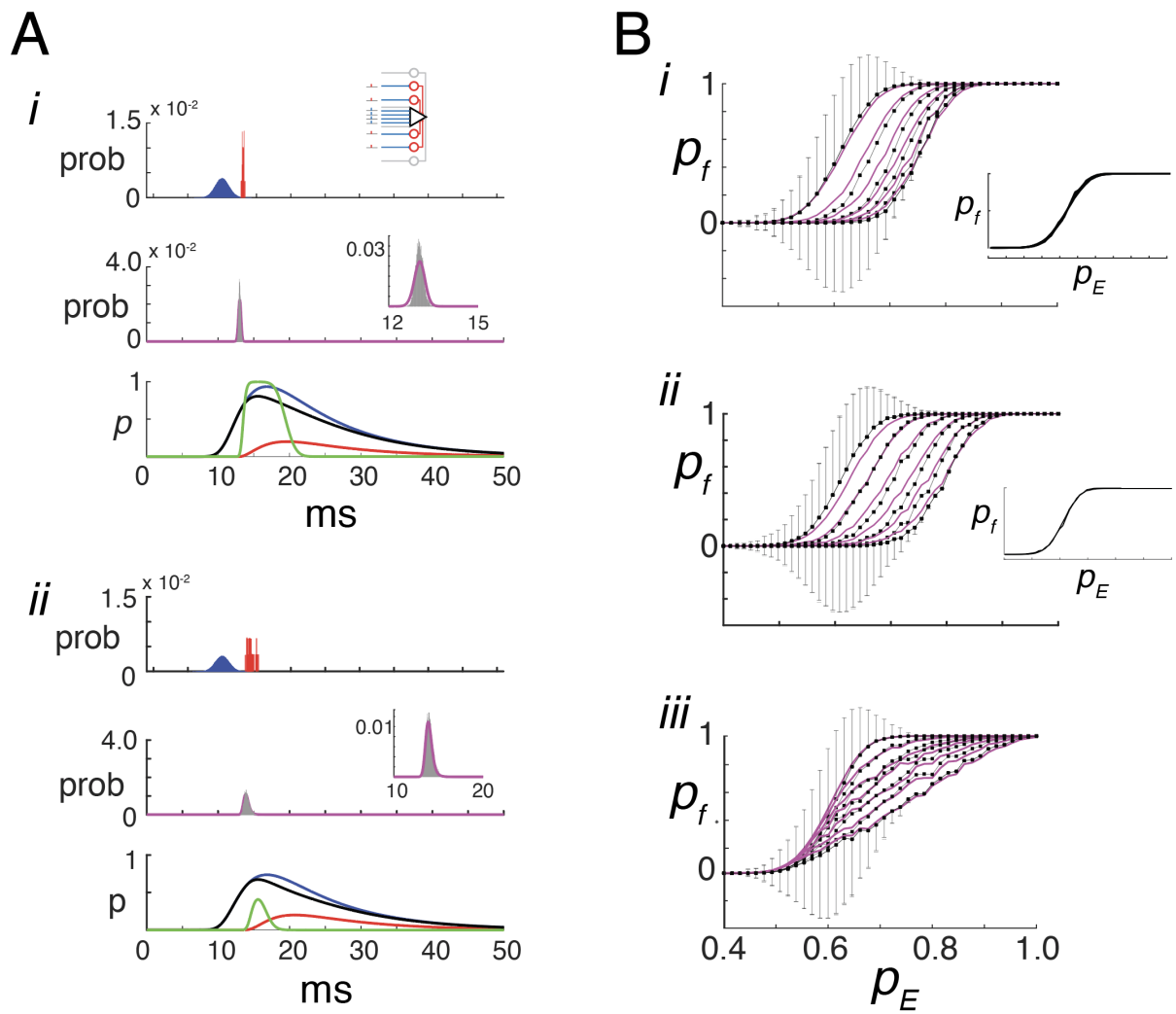

Figure 6: Predicting firing probability for transient stimuli. **A*i*,top**, probability distributions of arrival times of EPSP (blue) and IPSP (red) in the reference cell. **Middle**, predicted firing probability (magenta) overlaid on the spike time histogram (gray); **Inset**, magnified view. **Bottom**, superimposed traces of $\hat{p}_E(t)$ (blue), $\hat{p}_I(t)$ (red), net input $\hat{p}_{\text{net}}(t)$ (black), and threshold-crossing probability (green). **B,*i***, I-O curves showing mean firing probability (±SD) vs. p_E, for fixed p_I values ($0 \leq p_I \leq 0.5$). The p_I level was specified by adjusting and then fixing the input probability p_{EtoI}. Predicted values (magenta) are overlaid. Increasing p_I shifts the curve rightward without changing slope. **Inset**, I-O curves aligned by threshold. ***ii***, same but with p_I increasing linearly with p_E as $p_I = k_c p_E; 0 \leq k_c \leq 0.5$. ***iii***, same but with $p_{E \to I} = k_p p_E; 0.85 \leq k_p \leq 1$

The timing of action potentials is computed in two stages (see appendix S1). First, the probability that the net excitatory input at a given time exceeds the threshold required for firing was

computed from $\hat{p}_{\text{net}}$ (bottom, green curve; eq. S14). Second, this probability was used to derive the expected firing time (Eq. S15), accounting for the constraint that a neuron can fire only once and only if it has not already fired. This procedure yields the predicted firing probability (middle panel, magenta curve), which closely matches the spike histogram (gray, inset). Similar results were obtained for a weaker stimulus (Fig.6A,ii) and when the synaptic inputs were delivered as conductances (Fig.S3 in appendix S1).

Modulating inhibitory strength led to changes in the I-O curves that deviated from model predictions. Figure 6*i* shows the firing probability p_f plotted against p_E for different levels of p_I, analogous to the green curves in Fig.1B. The p_I level was controlled by adjusting and then fixing p_{EtoI} so that it, and hence p_I remained constant across values of p_E . As p_I increased, the firing threshold also increased, resulting in a rightward shift of the I–O curves , without a change in slope. When aligned by their respective thresholds, the curves collapsed onto a single profile (inset). Thus, unlike the toy model or the sustained input case, the effect on the I–O relationship was purely additive.

Similar results were obtained when p_I increased linearly with p_E ($p_I = k_c p_E$) (as in orange curve in Fig. 1B). With increasing k_c, the curves shifted to the right (*ii*), and was monotonic with no change in slope (inset). This occurred because the I did not cancel the E completely: a time window always existed between the onsets of $p_E(t)$ and $p_I(t)$ during which action potentials could be evoked. Thus, the effect on the I-O curve is also additive.

In Fig. 6B*(iii)*, inhibitory input probability p_I was modulated by varying the probability of excitatory inputs to inhibitory neurons, such that $p_{E\to I} = k_p p_E$. As in the case of the sustained stimulus condition (Fig. 3D, inset), the resulting p_I reflects the I–O function of the inhibitory (I) neurons, with the parameter k_p effectively controlling the threshold of inhibitory recruitment. As k_p increased, the slopes of the I–O curves of the reference cell decreased, while their thresholds remained constant. The thresholds did not change, and the curves remained monotonically increasing, again because of time window for excitation created by the lag in inhibition. Therefore, under these conditions, the effect on the I-O curve is multiplicative.

Discussion

This study aims to elucidate principles for computing stimulus-driven E -I interaction in feedforward inhibitory circuits. By combining E and I effects probabilistically, a straightforward relationship is derived that predicts changes in E -I balance during a stimulus. This framework links those changes to both cellular and network-level variables, providing insight into mechanisms that shape neuronal I–O curves, their modulation by inhibition, and overall response dynamics.

Combining E and I inputs probabilistically offers several theoretical advantages over traditional approaches that rely on summing synaptic currents to predict firing. First, the I-O curves are inherently rectified and sigmoidal -features that are often incorporated manually into models to prevent negative or unbounded firing rates [10, 19, 30, 59, 60, 61]. Second, this framework introduce synaptic noise naturally, producing smoothly rising I-O curves without requiring additional assumptions. Finally, the net probability (p_{net}) closely tracks the temporal firing patterns and can be used directly, or as input to Poisson point processes [62], to efficiently predict responses to stimuli.

Relation to previous work

The model's I-O curves exhibit two distinct regimes. For weak stimuli (low p_E), firing is in the sub-oscillatory regime and is driven primarily by input variability, producing a sigmoidal rise. This

behavior aligns with observations in visual cortex, where input summation is supralinear for weak stimuli and sublinear for strong ones [61, 63]. However, the underlying mechanisms may differ, as the visual responses are influenced by recurrent connectivity, which is absent in the current feedforward model. As input strength increases, the system enters an oscillatory regime, where the I–O curve may continue to rise, flatten, or become non-monotonic. The shape of the input-output (I-O) curve is determined by how inhibition scales with input, consistent with a previous model [19].

The model identifies key variables that shape the transformation of synaptic input into spiking output. Understanding this transformation has practical implications, as it may enable inference of intracellular dynamics from extracellular recordings [64]. While directly inverting the model equations is not possible due to the number of interacting variables (e.g., p_E, p_I, k_n, k_q, k_r), the derived relationships can still guide which parameters must be independently measured or constrained to yield reliable estimates.

Multiplicative gain modulation of I-O curves is important for maintaining tuning acuity across different cognitive states [27, 28, 65]. The current model reveals multiple mechanisms for achieving such modulation by altering how p_I scales with p_E (Fig. 3B–D). Unlike prior models [10, 30, 13], these effects emerge without relying on recurrent connectivity, synaptic noise, or conductance-based mechanisms. Moreover, the model may provide a framework for predicting neuromodulatory effects based on their actions on synaptic or biophysical parameters [66, 67].

The conditions for gain modulation differ between brief and prolonged stimuli. For brief stimuli, where firing is influenced by the delay between excitation and inhibition [4, 7, 49], multiplicative gain emerges only when changes in $\bar{p}_I$ with $\bar{p}_E$ follow the I–O curve of inhibitory neurons (Fig. 6B*iii*)—a scenario likely with natural stimuli. Optogenetic activation of inhibitory neurons during brief sensory stimulation [33] closely resembles simulations with fixed $\bar{p}_I$ (Fig. 6B*i*), which predict additive modulation of the I–O curves. The mixed multiplicative/additive effects observed experimentally may reflect the extent to which optogenetic stimulation overrides the normal physiological drive of the I neurons. For long duration stimuli, the model predicts that modulation is mostly multiplicative, which is consistent with optogenetic activation of inhibitory neurons during prolonged sensory stimulation [34].

The model reproduced many of the temporal firing patterns observed in cortical and subcortical regions [35, 36, 37, 38, 39, 46, 51] by adjusting the magnitude and timing of $p_E(t)$ and $p_I(t)$ (Fig. 5). One prediction is that transient firing and non-monotonic I-O curves observed experimentally [16, 35] may not necessarily arise from disproportionately large inhibitory drive. Both can occur even p_E and p_I increase in a balanced or proportional manner (Figs. 2B, 3C,D, 5). The model also shows that onset–offset responses can emerge when both $\bar{p}_E$ and $\bar{p}_I$ approach 1, with small changes in the inhibitory delay (Fig. 5). [42]. It remains unclear whether a similar mechanism operates in the cortex, as there is evidence that the onset and offset responses can be inherited from upstream subcortical regions [51, 40] and/or generated *de novo* [22, 41, 44].

Limitations

The theory is based on three key assumptions. The first is that calculation of p_{net} assumes inhibitory inputs sum linearly with and "cancel" out excitatory inputs. While the sublinear summation associated with conductance can be minimized with a correction term, the model does not account for heterogeneity in the size of the EPSPs and IPSPs. To simplify analyses, the size of the IPSPs were all expressed as a fraction of the EPSPs. However, the size of the PSPs depend on several factors including the location of the synapses and the identity of the presynaptic population. Thalamocortical synapses, for example, tend to be stronger than cortico-cortical synapses [68]. Moreover,

IPSPs at the soma can theoretically cancel many small EPSPs that originate in the distal dendrite via shunting.

Second, the constants (k_n, k_a, k_q, k_r) that scale p_I are chosen such that the product lies between 0 and 1, ensuring that p_I can be interpreted as a probability. In cortex, k_n $(= \frac{n_I}{n_E})$ is low ($\approx$ 0.15–0.20) [47, 48]. Excitatory and inhibitory synaptic current and potential amplitudes are generally comparable [8, 9, 69], suggesting that $k_a(= \frac{a_I}{a_E})$ and $k_q(= \frac{q_I}{q_E})$ is approximately 1. The shunting effect of inhibitory conductance is minimal for transient stimuli when the IPSP lags the EPSP, and can be compensated for during sustained stimulation. For prolonged stimuli, $k_r(= \frac{r_I}{r_E})$, could be large given the high firing rates of some interneurons [9, 69]. Moreover, k_q is likely to be dynamic, reflecting differential synaptic depression or facilitation of EPSPs and IPSPs [9, 53]. For practical modeling purposes, however, the product can be capped at 1.

Third, the model assumes that recurrent connections do not significantly contribute to the evoked firing rate. This may be valid for brief stimuli, as recurrent activity has a limited effect on firing [70]. In cortex, the connection probability between excitatory neurons is relatively low [9, 53]. Thus, if the active region is spatially restricted—as in tuned responses driven by topographically organized inputs—the small number of recruited local excitatory neurons would have minimal influence, consistent with simulation results [70]. Nonetheless, incorporating recurrent connectivity will be important for extending the model to more general cases.

Despite these limitations, the model effectively captures many key aspects of stimulus-evoked responses and can serve as a foundation for developing formal mathematical analyses [71] to study more complex network configurations.

Methods

The circuit consists of a reference neuron, whose firing activity serves as the model's output, and 20-50 local inhibitory neurons. Both cell types received 100-250 afferent from an excitatory source, with the reference cells also receiving inhibitory inputs from the interneurons. To control the E and I inputs to the reference cell, their afferents are treated independently. Thus, during a stimulus, the afferents evoked EPSPs in the reference cell occur with probability of p_E and in the I cells with probability $p_{E\to I}$. The number of I neurons is defined as a fraction of the total excitatory afferents: $n_I = k_n n_E; 0 \leq k_n \leq 1$. k_n is set to 0.2, unless stated otherwise.

Neurons are standard leaky-integrate-and-fire (LIF) neuron described by:

$$C\frac{dV}{dt} = -(\frac{(v - V_l)}{R} + i_E + i_I) \tag{6}$$

with resistance $R = 75$ MΩ, resting potential $V_l = -70mV$, membrane time constant $\tau_m = 10$ ms, the capacitance $C = \frac{\tau_m}{R}$, and action potential threshold = -55 mV.

The synaptic currents u_E, u_I are scaled alpha functions with $\tau = 2$ms,:

$$u_x(t) = a_x(t/\tau)e^{(1-t/\tau)};\ x \in \{E, I\} \tag{7}$$

where $a_E = 10.3, a_I = -10.3$ (in pA) for current clamp and $a_E = 0.147, a_I = 1.045$ (in nS) with $V_E = 0, V_I = -80$ (in mV) for conductance-based synapses. With these values, the excitatory and inhibitory postsynaptic potentials have amplitudes of 250 µV and -250 µV, respectively, at resting potential.

Transient stimuli

A histogram ($h_E(t)$) of arrival times of EPSPs to the reference and I neurons followed a Gaussian curve scaled by p_E : $h_E(t) = p_E\mathcal{N}(\mu_t, \sigma_t^2); \mu_t = 5$ ms, $\sigma_t = 0.1$ ms. This was convolved with $u_E(t)$ and delivered first to all the I neurons, each time with different realizations of $h_E(t)$. A time histogram $h_I(t)$ was compiled from the spikes evoked from the I cells. This was convolved with $u_I(t)$ and the current delivered to the reference cell along with excitatory current. This procedure was repeated $n_{trials} = 1000$-5000 times to compile spike histogram (Fig. 6A, middle panel, gray).

The p_I value was adjusted in 3 ways. First, p_I was held constant (Fig. 6Bi) by adjusting $p_{E\to I}$ until the desired p_I was attained; p_{EtoI} was then kept constant while p_E was varied. Second, to make p_I vary linearly with p_E (Fig. 6B,ii), p_I was scaled as $p_I = k_c p_E; k_c = k_n k_a$ while holding $p_{E\to I}$ at some constant value. Finally, to allow p_I to co-vary with stimulus intensity (Fig. 6Biii), $p_{E\to I}$ was varied linearly with p_E as $p_{E\to I} = k_p p_E$. The resulting p_I retained features of the inhibitory neurons' I-O curve: firing increased linearly after crossing a threshold.

The methods for calculating the time dependent probabilities and the predicted spike times are detailed in appendix S1.

Sustained stimuli

For sustained stimulus, excitatory synaptic barrages were generated by first creating a spike train using a Poisson process with rate $n_E r_E p_E(t)$ where $r_E = 50$ Hz is the average firing rate of a single afferent input from an external source and $n_E = 250$ is the number of afferents. The spike trains from $p_E(t)n_E$ afferents were compiled in a histogram and convolved with $u_E(t)$ to generate the excitatory input ($i_{exc}(t)$) to the reference and I neurons. $p_E(t)$ was ramped to a steady-state value and ramped back down to baseline, with the duration of the ramp ranging from 10 to 30 ms (Figs. 2). The excitatory barrage was delivered first to $n_I = 50$ inhibitory cells, and their evoked spikes compiled in a histogram $h_I(t)$.

The total number of inhibitory inputs received by the reference cell was calculated as $p_I k_q k_n k_r n_E$ where $k_q = |\frac{q_I}{q_E}| = 1, k_n = \frac{n_I}{n_E} = 0.2, k_r = \frac{r_I}{r_E}$ where q_E, q_I are the charges (set to 0.0557 pS and -0.0557 pS) generated by E and I inputs , respectively, and r_I is the firing rate evoked in inhibitory cells. These factored in $h_I(t)$, which was then convolved with $u_{inh}(t)$ to generate the inhibitory input $i_{inh}(t)$ to the reference cell. Both $i_{exc}(t)$ and $i_{inh}(t)$ were delivered to the reference cell ($n_{trials} = 1000 - 10000$) and the evoked response was used to calculate the average firing rate and the time histograms.

In some simulations (Figs. 5), the inhibitory neurons were bypassed. In these cases, the inhibitory input was calculated in the same way as the excitatory input and, after scaling, was delivered to the reference cell.

To examine how I-O curves depended on the magnitude of p_I (Figs. 3B-D), p_I was adjusted in 3 ways. First, to fix p_I at some specified value (Fig. 3B, inset), $p_{E\to I}$ was adjusted until the desired p_I was attained. $p_{E\to I}$ was then held constant while p_E was varied. Second, to make p_I vary linearly with p_E (Figs 3C, inset), $\bar{p}_I$was made to increase linearly with p_E as $\bar{p}_I = k_c p_E; 0 \leq k_c = k_n k_q k_r \leq 1$. In the simulations, k_c was varied by adjusting k_n and keeping k_r, k_q constant. Third, to make p_I co-vary with intensity (Fig. 3D, inset), p_{EtoI} increased with p_E as $p_{E\to I} = k_p p_E; 0 \leq k_p \leq 1$.

To examine gain modulation of receptive fields (Fig. 6), the tuned input was modeled as Gaussian function:

$$p_E(x) = ae^{-\frac{(x-x_{center})^2}{2\sigma_x}}$$

The $p_E(x)$ was then used to generate the drive to the reference cell and inhibitory neurons using the procedures described above.

References

[1] Harvey A Swadlow. "Thalamocortical control of feed–forward inhibition in awake somatosensory 'barrel'cortex". In: *Philosophical Transactions of the Royal Society of London. Series B: Biological Sciences* 357.1428 (2002), pp. 1717–1727.

[2] Michael Wehr and Anthony M Zador. "Balanced inhibition underlies tuning and sharpens spike timing in auditory cortex". In: *Nature* 426.6965 (2003), pp. 442–446.

[3] Scott J Cruikshank, Timothy J Lewis, and Barry W Connors. "Synaptic basis for intense thalamocortical activation of feedforward inhibitory cells in neocortex". In: *Nature neuroscience* 10.4 (2007), pp. 462–468.

[4] Laetitia Gabernet et al. "Somatosensory integration controlled by dynamic thalamocortical feed-forward inhibition". In: *Neuron* 48.2 (2005), pp. 315–327.

[5] Max L Schiff and Reyes. "Characterization of thalamocortical responses of regular-spiking and fast-spiking neurons of the mouse auditory cortex in vitro and in silico". In: *Journal of neurophysiology* 107.5 (2012), pp. 1476–1488.

[6] Sooyoung Chung, Xiangrui Li, and Sacha B Nelson. "Short-term depression at thalamocortical synapses contributes to rapid adaptation of cortical sensory responses in vivo". In: *Neuron* 34.3 (2002), pp. 437–446.

[7] Jeffry S Isaacson and Massimo Scanziani. "How inhibition shapes cortical activity". In: *Neuron* 72.2 (2011), pp. 231–243.

[8] Anne-Marie M Oswald and Reyes. "Maturation of intrinsic and synaptic properties of layer 2/3 pyramidal neurons in mouse auditory cortex". In: *Journal of neurophysiology* 99.6 (2008), pp. 2998–3008.

[9] Robert B Levy and Reyes. "Spatial profile of excitatory and inhibitory synaptic connectivity in mouse primary auditory cortex". In: *Journal of Neuroscience* 32.16 (2012), pp. 5609–5619.

[10] Frances S Chance, Larry F Abbott, and Alex D Reyes. "Gain modulation from background synaptic input". In: *Neuron* 35.4 (2002), pp. 773–782.

[11] Matteo Carandini. "Amplification of trial-to-trial response variability by neurons in visual cortex". In: *PLoS biology* 2.9 (2004), e264.

[12] Ian M Finn, Nicholas J Priebe, and David Ferster. "The emergence of contrast-invariant orientation tuning in simple cells of cat visual cortex". In: *Neuron* 54.1 (2007), pp. 137–152.

[13] Asli Ayaz and Frances S Chance. "Gain modulation of neuronal responses by subtractive and divisive mechanisms of inhibition". In: *Journal of neurophysiology* 101.2 (2009), pp. 958–968.

[14] Edward L Bartlett. "The organization and physiology of the auditory thalamus and its role in processing acoustic features important for speech perception". In: *Brain and language* 126.1 (2013), pp. 29–48.

[15] DP Phillips and DR Irvine. "Responses of single neurons in physiologically defined primary auditory cortex (AI) of the cat: frequency tuning and responses to intensity." In: *Journal of neurophysiology* 45.1 (1981), pp. 48–58.

[16] Benedikt Grothe. "Interaction of excitation and inhibition in processing of pure tone and amplitude-modulated stimuli in the medial superior olive of the mustached bat". In: *Journal of Neurophysiology* 71.2 (1994), pp. 706–721.

[17] Wensheng Sun et al. "Decoding sound level in the marmoset primary auditory cortex". In: *Journal of neurophysiology* 118.4 (2017), pp. 2024–2033.

[18] Andrew YY Tan et al. "Unbalanced synaptic inhibition can create intensity-tuned auditory cortex neurons". In: *Neuroscience* 146.1 (2007), pp. 449–462.

[19] Jorge F Mejias et al. "Subtractive, divisive and non-monotonic gain control in feedforward nets linearized by noise and delays". In: *Frontiers in computational neuroscience* 8 (2014), p. 19.

[20] Judith A Hirsch and Charles D Gilbert. "Synaptic physiology of horizontal connections in the cat's visual cortex". In: *Journal of Neuroscience* 11.6 (1991), pp. 1800–1809.

[21] Frédéric Pouille et al. "Input normalization by global feedforward inhibition expands cortical dynamic range". In: *Nature neuroscience* 12.12 (2009), pp. 1577–1585.

[22] IO Volkov and AV Galazjuk. "Formation of spike response to sound tones in cat auditory cortex neurons: interaction of excitatory and inhibitory effects". In: *Neuroscience* 43.2-3 (1991), pp. 307–321.

[23] Hysell Oviedo and Alex D Reyes. "Variation of input-output properties along the somatodendritic axis of pyramidal neurons". In: *Journal of Neuroscience* 25.20 (2005), pp. 4985–4995.

[24] Jérémie Barral and Reyes. "Synaptic scaling rule preserves excitatory–inhibitory balance and salient neuronal network dynamics". In: *Nature neuroscience* 19.12 (2016), pp. 1690–1696.

[25] David M Schneider, Janani Sundararajan, and Richard Mooney. "A cortical filter that learns to suppress the acoustic consequences of movement". In: *Nature* 561.7723 (2018), pp. 391–395.

[26] Pierre-Olivier Polack, Jonathan Friedman, and Peyman Golshani. "Cellular mechanisms of brain state–dependent gain modulation in visual cortex". In: *Nature neuroscience* 16.9 (2013), pp. 1331–1339.

[27] Carrie J McAdams and John HR Maunsell. "Effects of attention on orientation-tuning functions of single neurons in macaque cortical area V4". In: *Journal of Neuroscience* 19.1 (1999), pp. 431–441.

[28] Carrie J McAdams and R Clay Reid. "Attention modulates the responses of simple cells in monkey primary visual cortex". In: *Journal of Neuroscience* 25.47 (2005), pp. 11023–11033.

[29] Katie A Ferguson and Jessica A Cardin. "Mechanisms underlying gain modulation in the cortex". In: *Nature Reviews Neuroscience* 21.2 (2020), pp. 80–92.

[30] David J Heeger. "Normalization of cell responses in cat striate cortex". In: *Visual neuroscience* 9.2 (1992), pp. 181–197.

[31] Matteo Carandini and David J Heeger. "Summation and division by neurons in primate visual cortex". In: *Science* 264.5163 (1994), pp. 1333–1336.

[32] Nathan R Wilson et al. "Division and subtraction by distinct cortical inhibitory networks in vivo". In: *Nature* 488.7411 (2012), pp. 343–348.

[33] Bryan A Seybold et al. "Inhibitory actions unified by network integration". In: *Neuron* 87.6 (2015), pp. 1181–1192.

[34] Tina Gothner et al. "Sustained activation of PV+ interneurons in core auditory cortex enables robust divisive gain control for complex and naturalistic stimuli". In: *Cerebral Cortex* 31.5 (2021), pp. 2364–2381.

[35] Douglas McLelland et al. "Neuronal responses during and after the presentation of static visual stimuli in macaque primary visual cortex". In: *Journal of Neuroscience* 30.38 (2010), pp. 12619–12631.

[36] Paul D Cheney and Eberhard E Fetz. "Functional classes of primate corticomotoneuronal cells and their relation to active force". In: *Journal of neurophysiology* 44.4 (1980), pp. 773–791.

[37] Gregg H Recanzone. "Response profiles of auditory cortical neurons to tones and noise in behaving macaque monkeys". In: *Hearing research* 150.1-2 (2000), pp. 104–118.

[38] Ling Qin et al. "Neural and behavioral discrimination of sound duration by cats". In: *Journal of Neuroscience* 29.50 (2009), pp. 15650–15659.

[39] Bettina Joachimsthaler et al. "Quantitative analysis of neuronal response properties in primary and higher-order auditory cortical fields of awake house mice (M us musculus)". In: *European Journal of Neuroscience* 39.6 (2014), pp. 904–918.

[40] Ben Scholl, Xiang Gao, and Michael Wehr. "Nonoverlapping sets of synapses drive on responses and off responses in auditory cortex". In: *Neuron* 65.3 (2010), pp. 412–421.

[41] Magdalena Solyga and Tania Rinaldi Barkat. "Emergence and function of cortical offset responses in sound termination detection". In: *Elife* 10 (2021), e72240.

[42] Conny Kopp-Scheinpflug, James L Sinclair, and Jennifer F Linden. "When sound stops: offset responses in the auditory system". In: *Trends in neurosciences* 41.10 (2018), pp. 712–728.

[43] O Creutzfeldt, F-C Hellweg, and Chr Schreiner. "Thalamocortical transformation of responses to complex auditory stimuli". In: *Experimental brain research* 39.1 (1980), pp. 87–104.

[44] Giulio Bondanelli et al. "Network dynamics underlying OFF responses in the auditory cortex". In: *Elife* 10 (2021), e53151.

[45] Xiaoqin Wang et al. "Sustained firing in auditory cortex evoked by preferred stimuli". In: *Nature* 435.7040 (2005), pp. 341–346.

[46] Douglas McLelland, Bashir Ahmed, and Wyeth Bair. "Responses to static visual images in macaque lateral geniculate nucleus: implications for adaptation, negative afterimages, and visual fading". In: *Journal of Neuroscience* 29.28 (2009), pp. 8996–9001.

[47] Daniel Maxim Iascone et al. "Whole-neuron synaptic mapping reveals spatially precise excitatory/inhibitory balance limiting dendritic and somatic spiking". In: *Neuron* 106.4 (2020), pp. 566–578.

[48] Clermont Beaulieu. "Numerical data on neocortical neurons in adult rat, with special reference to the GABA population". In: *Brain research* 609.1-2 (1993), pp. 284–292.

[49] AYY Tan and M Wehr. "Balanced tone-evoked synaptic excitation and inhibition in mouse auditory cortex". In: *Neuroscience* 163.4 (2009), pp. 1302–1315.

[50] Stefan Treue and Julio C Martinez Trujillo. "Feature-based attention influences motion processing gain in macaque visual cortex". In: *Nature* 399.6736 (1999), pp. 575–579.

[51] Ling Qin et al. "Comparison between offset and onset responses of primary auditory cortex ON–OFF neurons in awake cats". In: *Journal of neurophysiology* 97.5 (2007), pp. 3421–3431.

[52] Haifu Li et al. "Phasic Off responses of auditory cortex underlie perception of sound duration". In: *Cell reports* 35.3 (2021).

[53] Luke Campagnola et al. "Local connectivity and synaptic dynamics in mouse and human neocortex". In: *Science* 375.6585 (2022), eabj5861.

[54] Scott J Cruikshank, Heather J Rose, and Raju Metherate. "Auditory thalamocortical synaptic transmission in vitro". In: *Journal of neurophysiology* 87.1 (2002), pp. 361–384.

[55] Michael Beierlein, Jay R Gibson, and Barry W Connors. "Two dynamically distinct inhibitory networks in layer 4 of the neocortex". In: *Journal of neurophysiology* 90.5 (2003), pp. 2987–3000.

[56] Zhenjun Tan et al. "Robust but delayed thalamocortical activation of dendritic-targeting inhibitory interneurons". In: *Proceedings of the National Academy of Sciences* 105.6 (2008), pp. 2187–2192.

[57] Yi Zhou et al. "Preceding inhibition silences layer 6 neurons in auditory cortex". In: *Neuron* 65.5 (2010), pp. 706–717.

[58] Judith A Hirsch et al. "Synaptic integration in striate cortical simple cells". In: *Journal of neuroscience* 18.22 (1998), pp. 9517–9528.

[59] Hugh R Wilson and Jack D Cowan. "Excitatory and inhibitory interactions in localized populations of model neurons". In: *Biophysical journal* 12.1 (1972), pp. 1–24.

[60] Brent Doiron et al. "Subtractive and divisive inhibition: effect of voltage-dependent inhibitory conductances and noise". In: *Neural computation* 13.1 (2001), pp. 227–248.

[61] Daniel B Rubin, Stephen D Van Hooser, and Kenneth D Miller. "The stabilized supralinear network: a unifying circuit motif underlying multi-input integration in sensory cortex". In: *Neuron* 85.2 (2015), pp. 402–417.

[62] Peter Dayan and Laurence F Abbott. *Theoretical neuroscience: computational and mathematical modeling of neural systems*. MIT press, 2005.

[63] Kenneth D Miller and Todd W Troyer. "Neural noise can explain expansive, power-law nonlinearities in neural response functions". In: *Journal of neurophysiology* 87.2 (2002), pp. 653–659.

[64] Ryota Kobayashi and Shigeru Shinomoto. "Inference of monosynaptic connections from parallel spike trains: a review". In: *Neuroscience Research* (2024).

[65] Kenneth D Harris and Alexander Thiele. "Cortical state and attention". In: *Nature reviews neuroscience* 12.9 (2011), pp. 509–523.

[66] Tingting Liu, Iraklis Petrof, and S Murray Sherman. "Modulatory effects of activation of metabotropic glutamate receptors on GABAergic circuits in the mouse cortex". In: *Journal of Neurophysiology* 111.11 (2014), pp. 2287–2297.

[67] Carmen Varela. "Thalamic neuromodulation and its implications for executive networks". In: *Frontiers in neural circuits* 8 (2014), p. 69.

[68] Ziv Gil, Barry W Connors, and Yael Amitai. "Efficacy of thalamocortical and intracortical synaptic connections: quanta, innervation, and reliability". In: *Neuron* 23.2 (1999), pp. 385–397.

[69] Anne-Marie M Oswald and Reyes. "Development of inhibitory timescales in auditory cortex". In: *Cerebral Cortex* 21.6 (2011), pp. 1351–1361.

[70] Robert B Levy and Reyes. "Coexistence of lateral and co-tuned inhibitory configurations in cortical networks". In: *PLoS computational biology* 7.10 (2011), e1002161.

[71] Alex D Reyes. "Mathematical framework for place coding in the auditory system". In: *PLoS computational biology* 17.8 (2021), e1009251.

1 S1 Appendix

Correcting for conductance

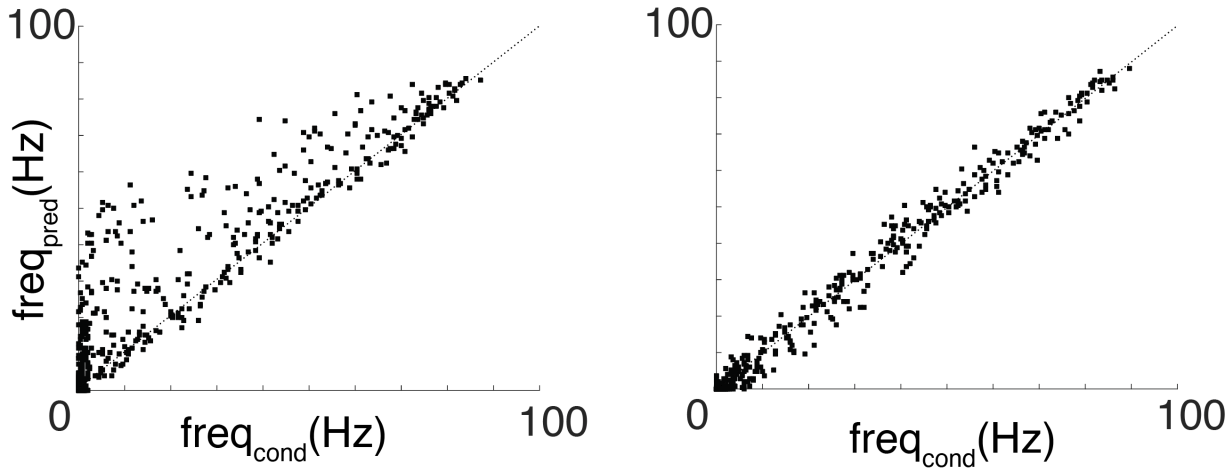

Figure 1: Effects of conductance. **Left**, plot of predicted firing assuming the PSPs summed linearly vs firing rate evoked with conductance-based synapses. **Right**, same but with correction term for voltage-dependent non-linear summation of PSPs.

The voltage-dependent unitary postsynaptic current for E and I are, respectively, $\mu_E(v,t) = g_E(t)(v - V_{exc})$ and $\mu_I(v,t) = g_I(t)(v - V_{inh})$, where the g's are conductances and the V's are the equilibrium potentials. The voltage-dependent charges are therefore:

$$\begin{aligned} q_E(v) &= (v - V_{exc}) \cdot \int g_E(t)dt \ (\frac{coul}{V - sec}) \\ &= G_E \cdot (v - V_{exc}) \\ q_I(v) &= (v - V_{inh}) \cdot \int g_I(t)dt \\ &= G_I \cdot (v - V_{inh}) \end{aligned} \tag{1}$$

The voltage-dependent synaptic current barrages are then given by:

$$
\begin{aligned}
i_E(v) &= p_E r_E n_E G_E \cdot (v - V_{exc}) \qquad (2)\\
i_I(v) &= p_E p_I r_I n_E G_I \cdot (v - V_{inh})\\
i_{net}(v) &= p_E r_E n_E G_E \cdot (v - V_{exc}) + p_E p_I r_I n_I G_I \cdot (v - V_{inh})\\
&= p_E r_E n_E G_E (v - V_{exc}) + p_E p_I k_r r_E k_n n_E k_g G_E (v - V_{inh}); k_g = \frac{G_I}{G_E}\\
&= r_E n_E G_E [(p_E \cdot (v - V_{exc}) + p_E p_I k_r k_n k_g (v - V_{inh})]\\
&= r_E n_E G_E [p_E \cdot (v - V_{exc}) + p_E p_I k_r k_n k_g (\frac{v - V_{inh}}{v - V_{exc}})(v - V_{exc})]\\
&= r_E n_E G_E [(p_E (v - V_{exc}) - p_E p_I k_r k_n k_g (-(\frac{v - V_{inh}}{v - V_{exc}}))(v - V_{exc})]\\
&= r_E n_E G_E [(p_E (v - V_{exc}) - p_E p_I k_r k_n k_g k_v (v - V_{exc})]; k_v = -(\frac{v - V_{inh}}{v - V_{exc}})\\
&= r_E n_E G_E \cdot (v - V_{exc})[(p_E - p_E p_I k_r k_n k_g k_v]\\
&= r_E n_E G_E \cdot (v - V_{exc}) p_{net}
\end{aligned}
$$

under the restriction that $0 \leq k_r k_n k_g k_v \leq 1$.

To examine how non-linear summation affects the predicted firing, simulations were performed as described in the main text (Methods), but with synaptic inputs modeled as conductances rather than current. To ensure equal amplitudes ($250\mu V$ for EPSPs, $-250\mu V$ for IPSPs) at resting potential (-70 mV) and with the excitatory and inhibitory reversal potentials of 0 and -80 mV, the inhibitory conductance needed to be 7 times larger than the excitatory conductance. The resulting firing rate ($freq_{cond}$) was compared to that predicted ($freq_{pred}$) when the E and I inputs were first combined using eq. 2, assuming linear summation of synaptic currents without voltage dependence, and then delivered to the reference cell as i_{net}. To explore the firing rates under different conditions, the simulations were performed with a random combinations of p_E (ranging from 0.6 to 1; 0.6 is minimum to evoke firing), p_{EtoI} (0.5 to 1), and ratio k_n (0.2 to 1) across 1000 trials. Plotting the frequencies against each other (Fig. S 2) (left) shows that $freq_{pred}$ overestimated $freq_{cond}$, as many of the points lie above the unitary slope line (dotted). Adding the correction term improved the match significantly (right).

Generation of bimodal tuning curves

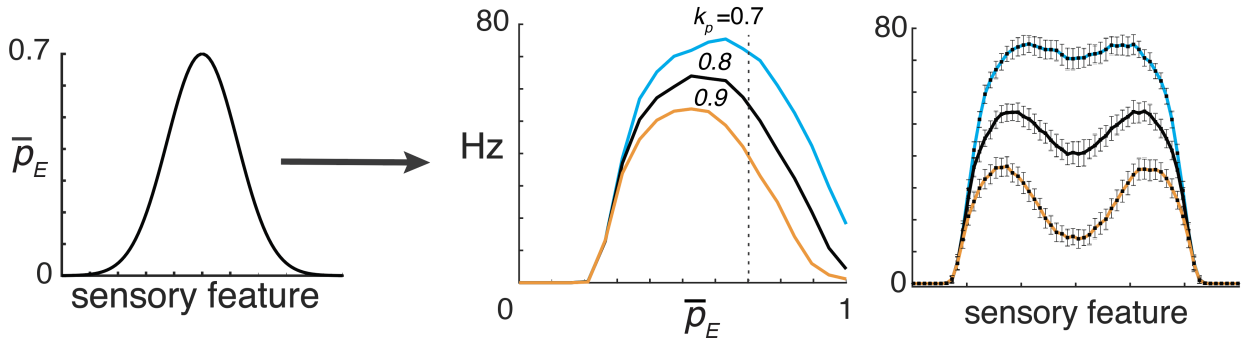

Figure 2: Effects of large tuned input. **Left**, tuned input with peak of 0.7. **Middle**, I-O curves obtained when $p_{E\to I}$ increased with p_E as $p_{E\to I} = k_p p_E$ $p_{E\to I}$. **Right**, tuned responses showed a dip at the center .

In Fig. 4D of the main text, simulations were performed with small amplitude tuning curve (peak =0.35) under the condition that $p_{E\to I}$ increased linearly with p_E . With this amplitude, the firing fell on the rising edge of the I-O curves and multiplicative gain modulation was produced. In Fig.S2, the amplitude of the tuned input was doubled to 0.7. Because the evoked firing corresponded to the decaying edge of the I-O curves (middle), the tuned responses (right) had a dip at the center.

Effects of conductance for brief stimuli

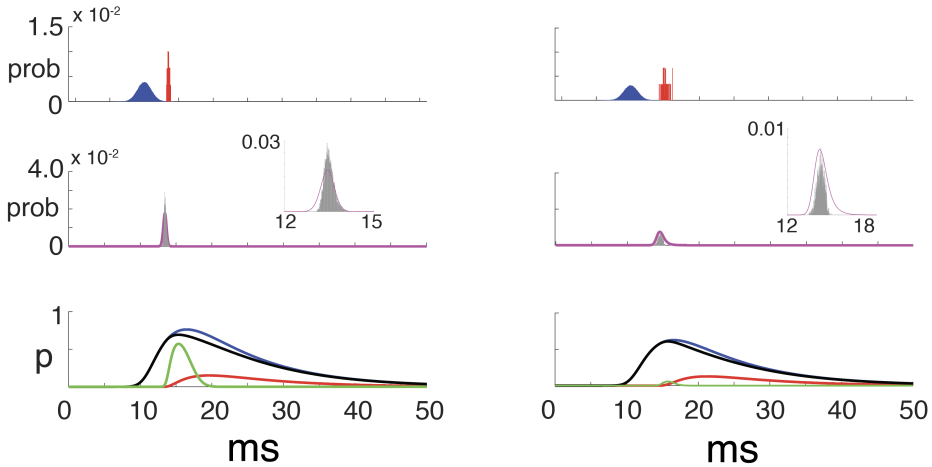

Figure 3: Predicting firing probability for transient stimuli with conductance. Simulation performed with synaptic input delivered as conductances. **Left** ,top histograms showing arrival times of EPSPs (blue) and IPSPs (red) in the reference cell. Middle, predicted firing probability (magenta) superimposed on histogram of evoked action potentials in reference cell (gray). Inset, close up of histogram. Bottom, time courses of $\hat{p}_E$ (blue), $\hat{p}_I$ (red), and $\hat{p}_{net}$ (black). The probability that the membrane potential exceeds threshold for firing is shown in green. **Right**, same but with weaker input.

Simulations with brief stimuli and synaptic conductances

The simulations conducted in the main text with transient stimuli assumed linear summation of synaptic inputs. However, there are scenarios where summation may be sublinear, such as when synapses are in close proximity or when inhibition causes significant shunting. To assess whether the model holds under these conditions, simulations were performed using conductance-based synaptic inputs (see Methods). Figure S3 shows that the results were qualitatively similar to those from the linear model (compare with Fig. 6 in the main text). The effects of conductance were not more pronounced, partly because action potentials occur primarily on the rising edge of $p_E(t)$ (compare the middle and bottom traces), before significant overlap with $p_I(t)$ occurs.

Derivation and overview of model scope and parameters

The network is configured as feedforward inhibitory circuit, receiving excitatory inputs from an external source. It consists of a reference neuron and $n_I = 20 - 50$ inhibitory neurons, each receiving $n_E = 100 - 250$ external inputs; the reference neuron also receives inputs from the local inhibitory neurons. In response to a stimulus, excitatory inputs from the external source arrive at the reference and inhibitory cells with probability p_E and $p_{E\to I}$, respectively. When the inhibitory cells fire, inhibitory inputs arrive at the reference cell with probability p_I. The amplitudes of the excitatory and inhibitory inputs are designated as a_E, a_I in mV (but also as q_E, q_I in coulombs). The relative number and size of the excitatory and inhibitory inputs may be expressed with proportionality constants: $n_I = k_n n_E; k_n \geq 0$ and $a_I = -k_a a_E; k_a \geq 0$.

A key feature of the model is that the inhibitory inputs that are functionally relevant are those that appear at the same time as the excitatory inputs during the stimulus. When this happens, the excitatory input is effectively "canceled." This interaction is represented by the product $p_E p_I$, assuming independence. This reflects the reduction in the purely excitatory probability due to inhibition, which can be expressed as the net probability: $p_{net} = p_E - p_E p_I = p_E(1 - p_I)$. There are two important consequences or conditions:

1. As formulated, $0 \leq p_{net} \leq 1$, which is a requirement for probability. This condition must be maintained as p_I is multiplied by various constants to account for network size and input amplitudes.

2. The total number of active afferents n_{act} is always greater than or equal to 0 ($n_{act} \geq 0$). In the absence of inhibition, the number of afferents that are activated is $n_{act} = p_E n_E$. With inhibition, the net number of uncanceled excitatory inputs is:

$$\begin{aligned} n_{act} &= n_E p_E - n_I p_E p_I \\ &= n_E p_E - k_n n_E p_E p_I \\ &= n_E p_E (1 - k_n p_I) \\ &= n_E p_{net} \end{aligned} \tag{3}$$

To ensure that $0 \leq p_I, p_{net} \leq 1$, $0 \leq k_n \leq 1$. That is, under this condition, the number of inhibitory neurons must be less than or equal to the number of excitatory afferents.

In the following sections, these relationships are adjusted in different ways to apply them to various stimulus scenarios.

1. Calculating firing probability with transient input

The following refers to a reference neuron that receives n_E excitatory inputs from an external source and n_I inhibitory inputs from local inhibitory interneurons, with for the moment, no delay in the arrival of EPSPs and IPSPs. The EPSPs and IPSPs evoked from the external afferents and inhibitory interneurons, respectively, are small. In the presence of a stimulus, the EPSPs from the afferents appear in the reference cell and in the local interneurons with probabilities p_E and $p_{E\to I}$, respectively. The interneurons will fire with probability of p_I , either as a result of the external stimulus and/or some background activity.

In the presence of the stimulus, an average of $n_E p_E$ excitatory inputs appear in the reference cell. Of the $n_I p_I$ inhibitory inputs that arrive in the reference cell, $p_E n_I p_I$ will arrive at the same time as the excitatory inputs. Thus, the net (or uncancelled) number of excitatory inputs is $n_{net} = n_E p_E - p_E n_I p_I$. If the amplitude (in mV) of the EPSP is a_E and that of the IPSP is a_I, the average amplitude of the combined PSPs with the scaling factors k_n, k_a (see above) is:

$$
\begin{aligned}
a_{net} &= n_E p_E a_E - p_E n_I p_I a_I \\
&= n_E p_E a_E - p_E k_n n_E p_I k_a a_E; 0 \leq k_n k_a \leq 1 \\
&= n_E a_E p_E (1 - k_n k_a p_I) \\
&= n_E a_E p_{net}
\end{aligned} \tag{4}
$$

The probability of evoking an action potential is the probability that a_{net} exceeds threshold for firing v_θ or, equivalently, the probability that the net number of EPSPs exceed the minimum threshold number ($n_\theta = \frac{v_\theta}{a_E}$). The firing probability is then calculated from the cumulative binomial distribution (β):

$$
\begin{aligned}
p_f &= prob(n_{net} \geq n_\theta) = 1 - \beta(n_E, n_\theta, p_{net}) \\
\beta &= \sum_{i=0}^{n_\theta} \binom{n_E}{i} p_{net}(t)^i (1 - p_{net}(t))^{n_E - i}
\end{aligned} \tag{5}
$$

The next step is to derive a more general form that relaxes the assumption that the E and I inputs arrive simultaneously. A brief stimulus evokes a composite EPSP ($C_E(t)$) and the accompanying composite IPSP ($C_I(t)$). The composite PSPs is formed by multiple unitary PSPs (i.e. the amplitude of a PSP from a single external or inhibitory axon) and the average is given by:

$$
\begin{aligned}
C_E(t) &= p_E a_E n_E \mu(t) \\
C_I(t) &= p_I a_I n_I \mu(t) \\
&= -p_I k_a a_E k_n n_E \mu(t); \text{ since } a_I \text{ is negative} \\
&= -a_E n_E (k_a k_n p_I) \mu(t), 0 \leq k_a k_n \leq 1
\end{aligned} \tag{6}
$$

where $u(t)$ is the time course of the unitary PSP (alpha function; see Methods) with peak amplitude of 1. The summed composite, with inhibition conditioned on appearing at the same time as the EPSP, is then:

$$
\begin{aligned}
C_{tot}(t) &= p_E a_E n_E \mu(t) - p_E p_I k_a a_E k_n n_E \mu(t) \\
&= a_E n_E \mu(t)(p_E - p_E(k_a k_n p_I) \\
&= a_E n_E \mu(t) p_E (1 - k_a k_n p_I) \\
&= a_E n_E \mu(t) p_{net}
\end{aligned} \tag{7}
$$

If the arrival times of the excitatory inputs are jittered and Normally-distributed over time (denoted as $\mathcal{N}(\mu_t, \sigma_t^2)$ with u_t and σ_t the mean and standard deviation, respectively) , the histogram of arrival times of the excitatory input is

$$
h_E(t) = n_E p_E \mathcal{N}(\mu_t, \sigma_t^2) \tag{8}
$$

The histogram $h_I(t)$ for the arrival times of inhibition is empirically measured from the activities of the n_I inhibitory cells and can be re-written as:

$$
\begin{aligned}
h_I(t) &= n_I p_I \mathcal{P}_I \\
&= k_n n_E p_I \mathcal{P}_I
\end{aligned} \tag{9}
$$

where $\mathcal{P}_I$ is a probability distribution.

The composite EPSPs and IPSPs are obtained by the convolutions:

$$\begin{aligned} C_E(t) &= a_E \int h_E(t-\tau) * u(\tau) d\tau \\ &= a_E n_E p_E \int \frac{1}{n_E p_E} h_E(t-\tau) * u(\tau) d\tau \\ &= a_E n_E p_E \phi_E(t) \\ &= a_E n_E \hat{p}_E(t) \\ C_I(t) &= -a_I \int h_I(t-tau) * u(\tau) d\tau \\ &= -a_I k_n n_E p_I \int \frac{1}{k_n n_E p_I} h_I(t-\tau) * u(\tau) d\tau \\ &= -k_a a_E k_n n_E p_I \phi_I(t); 0 \leq k_a k_n \leq 1 \\ &= -k_a a_E k_n n_E \hat{p}_I(t) \end{aligned} \tag{10}$$

The summed composite is then:

$$\begin{aligned} C_{tot}(t) &= a_E n_E p_E \phi_E(t) - k_a a_E k_n n_E p_I \phi_I(t) \\ &= a_E n_E \hat{p}_E(t) - k_a a_E k_n n_E \hat{p}_I(t) \end{aligned} \tag{11}$$

Following the reasoning in the main text, the inhibitory component can only exert its effect if the membrane potential at some time t has an EPSP component. Therefore, we may define:

$$\begin{aligned} \hat{p}_{net}(t) &= \hat{p}_E(t) - \hat{p}_E(t) k_a k_n \hat{p}_I(t) \\ &= \hat{p}_E(t)(1 - k_a k_n \hat{p}_I(t)) \end{aligned} \tag{12}$$

The effective composite PSP is then:

$$C_{eff}(t) = a_E n_E \hat{p}_E(t)(1 - k_a k_n \hat{p}_I(t)) \tag{13}$$

The probability that the cell will fire is equal to the probability that the voltage at a given time exceeds the action potential threshold v_θ. Alternatively, this is equal to the probability that the net number of excitatory inputs $n_{net}(t)$ at a given time exceeds the minimum number n_θ needed to cross threshold. The probability of firing is then:

$$p_f(t) = prob(n_{net}(t) \geq n_\theta) = (1 - \beta(n_\theta, n(t), \hat{p}_{net})) \tag{14}$$

where β is the binomial cumulative distribution function (green curve in Fig. 6 A, bottom panel of main text).

Finally, the probability that the action potential will occur at a specific time t_i is equal to the probability of firing at time t_i $(= p_f(t_i))$ multiplied by the probability that it didn't occur at earlier times $(p_f(t_{i-1})p_f(t_{i-2}), \dots)$.

$$prob(\text{spike at } t_i) = p_f(t_i)\pi_{j=1}^{i-1}(1 - p_f(t_j)) \tag{15}$$

This is the magenta curve in Fig.6A, middle panel.

2. Calculating firing probability with sustained input

Many neurons, in response to sustained synaptic input, enter the oscillatory firing regime. Typically, the firing rate depends on the mean synaptic current (so-called firing rate-current, or f-I curve). During a sustained stimulus, the afferents and I neurons trains of EPSPs and IPSPs, respectively, producing a synaptic barrage in the postsynaptic neuron.

We define $p_E(t)$ as the time-varying probability that an afferent will fire and generate a train of EPSPs in the reference cell for each stimulus. Each train has an average rate r_E and lasts for some period of time. Therefore, the fraction of the total afferents (n_E) activated is $p_E n_E$ and the excitatory current, assuming each afferent fires independently of the others is then:

$$i_E(t) = p_E(t) n_E q_E r_E \tag{16}$$

where q_E is the charge generated by a single afferent (=area under synaptic current) and r_E is the average firing rate.

The stimulus also generates synaptic current in the n_I inhibitory neurons, causing them to fire with probability $p_I(t)$. Assuming for simplicity that the I cell firing is independent of the afferent firing, the probability that the I firing will coincide with the afferent firing is therefore $p_E(t) \cdot p_I(t)$. When an I cell becomes active, it generates a train of IPSPs and so for n_I neurons, and the inhibitory current (under the condition that the inhibitory input coincides with the excitatory) to the reference cell is:

$$i_I(t) = -p_E(t) \cdot p_I(t) n_I q_I r_I \tag{17}$$

The net current is:

$$\begin{aligned} i_{net}(t) &= p_E(t) \cdot (n_E q_E r_E - p_I n_I q_I r_I) \\ &= n_E q_E r_E p_E(t) \cdot (1 - k_n k_q k_r p_I(t)); \; 0 \leq k_n k_q k_r \leq 1 \\ &= n_E q_E r_E p_{net}(t) \end{aligned} \tag{18}$$

where $k_n = \frac{n_I}{n_E}, kq = |\frac{q_I}{q_E}|, k_r = \frac{r_I}{r_E}$.

The evoked firing rate in the oscillatory regime is then calculated by:

$$r_{osc}(t) = S(\bar{i}_{net}(t)) \tag{19}$$

where S is an input-output function (e.g. experimentally measured f-I curve), a model neuron, or in the case of an LIF neuron as $[(\tau_m * ln(\frac{\bar{i}_{net}}{\bar{i}_{net} - i_{rh}})]^{-1}$ where $\bar{i}_{net}$ is the average net current and i_{rh} is the rheobase or minimum current needed to evoke firing.

In the sub-oscillatory regime, spurious firing occurs because of variability that causes the synaptic current i_{syn} to exceed rheobase. This probability is given by:

$$\begin{aligned} prob(\bar{i}_{net} > i_{rh}) &= 1 - prob(\bar{i}_{net} \leq i_{rh}) \\ &= 1 - prob(n \leq n_\theta) = (1 - \beta(n_E, n_\theta, p_{net}(t))) \end{aligned} \tag{20}$$

where β is the binomial cumulative distribution function and n_θ is the minimum number of excitatory afferents needed to achieve rheobase. This function saturates to 1 at close to the start of the oscillatory regime. Scaling the function by the minimum evoked firing in the oscillatory regime (r_{rh}) joins the curves at the two regimes. The firing rate is defined to be the larger of the two:

$$r_{fluct} = r_{rh}(1 - \beta(n_E, n_\theta, p_{net}(t))) \tag{21}$$
$$r_f = max(r_{fluct}, r_{osc})$$

.